Direct Current Electric Field Assembly of Colloidal Crystals Displaying Reversible Structural Color

Aayush A. Shah,[†] Mahesh Ganesan,[‡] Jennifer Jocz,[‡] and Michael J. Solomon[†,‡,*]

[†]Macromolecular Science and Engineering and [‡]Chemical Engineering, University of Michigan, Ann Arbor, Michigan 48109, United States

ABSTRACT We report the application of low-voltage direct current (dc) electric fields to self-assemble close-packed colloidal crystals in nonaqueous solvents from colloidal spheres that vary in size from as large as 1.2 μm to as small as 0.1 μm. The assemblies are created rapidly (~2 min) from an initially low volume fraction colloidal particle suspension using a simple capacitor-like electric field device that applies a steady dc electric voltage. Confocal microscopy is used to observe the ordering that is produced by the assembly method. This spatial evidence for ordering is consistent with the 6-fold diffraction patterns identified by light scattering. Red, green, and blue structural color is observed for the ordered assemblies of colloids with diameters of 0.50, 0.40, and 0.29 μm, respectively, consistent with spectroscopic measurements of reflectance. The diffraction and spectrophotometry results were found to be consistent with the theoretical Bragg's scattering expected for closed-packed crystals. By switching the dc electric field from on to off, we demonstrate reversibility of the structural color response on times scales ~60 s. The dc electric field assembly method therefore represents a simple method to produce reversible structural color in colloidal soft matter.

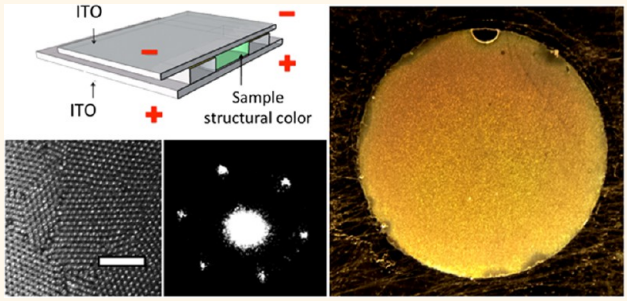

KEYWORDS: electric field assembly · colloidal crystal · structural color · diffraction · Bragg's law · reversibility · functional colloidal assemblies

Spatial ordering at the micrometer and submicrometer scale is responsible for the distinctive optical and photonic properties found in nature, such as the brilliant, iridescent colors of butterfly wings[1] and beetles[2] as well as the camouflage of cephalopods.[3] Similar periodically ordered features at the submicrometer and micrometer scale have been produced through top-down fabrication as well as through the self-assembly of synthetic colloidal spheres.[4] Pusey and van Megen formed iridescent colors by equilibrium self-assembly of nearly refractive index-matched colloidal spheres into highly ordered, nearly close-packed crystalline phases.[5] However, the self-assembly of colloidal particles is both a slow process and one prone to dislocations, vacancies, and grain boundaries that reduce the quality of the colloidal crystals. Surface templating can improve crystal quality,[6,7] while methods such as spin coating[8,9] and convective assembly[10−13] can significantly enhance assembly rates as well as uniformity. These methods give permanent crystals that have a uniform color similar to that observed in nature. This structural color obtained from colloidal crystals can be tuned by embedding synthesized colloidal crystals into elastomers and polymers.[14] The elastomers change the color properties of the material by tuning the lattice arrangement of the embedded colloidal crystal by stretching and contracting in response to stimuli such as mechanical stress,[15] pH changes,[16] and electric actuation.[17]

These methods are thus available to create permanent colloidal crystals with static crystalline microstructure. On the other hand, external fields can be used to tune the order−disorder transition and thus the microstructure of colloidal particle assemblies. External fields such as alternating current (ac) electric fields,[18,19] centrifugation,[20] magnetic fields,[21−23] and light[24] are increasingly used to control forces and thus the assembly of colloidal particles.

* Address correspondence to mjsolo@umich.edu.

Received for review April 16, 2014 and accepted August 5, 2014.

Published online August 05, 2014
10.1021/nn502107a

In most cases, application of external fields generates reversible close-packed assemblies of colloidal particles. For example, ac electric fields can assemble colloidal particles into ordered structures that dissipate into a disordered fluid phase on removal of the ac electric field.[18,25−28] However, these field-driven methods require auxiliary equipment (ac electric fields and centrifugation) and specialized colloidal particles (magnetic materials) and/or have slow 3D assembly times (centrifugation).

The application of direct current (dc) electric fields is a promising method to address the need for rapid, reversible assembly of colloids by a simple process. Such electrophoretic deposition of colloidal particles has been used to create two-dimensional disordered aggregates[29] as well as ordered crystalline assemblies.[30−32] These methods deploy electrochemically active solvents (typically water) that react at the electrode, thereby generating electroosmotic or electrohydrodynamic flows that drive colloidal assembly on a planar electrode.[31,33,34] The surface flows associated with these dc electric field assembly methods largely limit their application to planar assemblies of colloids.

However, recent reports of successful assembly of colloids into three-dimensional colloidal crystals by means of dc electric fields have renewed interest in this assembly method.[35,36] The difference between these new methods and prior work is the use of nonaqueous solvents such as dimethyl sulfoxide (DMSO), ethanol, and mixtures of cyclohexyl bromide and decalin (CHB/decalin). In this way, Rogach *et al.* have shown that dried ordered films that possess bulk optical properties can be made from colloidal particles.[35] Shah *et al.* have shown that even ellipsoidal (rod-shaped) particles can be assembled into high volume fraction crystal structures.[36] The advance of these studies is that replacing the aqueous solvent with a nonaqueous one appears to reduce the rate of solvent decomposition reactions at the electrode, thereby ameliorating the strength of electrohydrodynamic flows that generated the prior limitation to 2D assemblies. In its place, low-rate electrochemical reactions of dissolved residual reactants (such as oxygen, surfactants, or water) create an $\sim 0.1-5\ \mu A/cm^2$ current that drives electrophoretic deposition of colloids that are charged in the carrier solvent.

In this paper, we exploit the electrophoretic deposition effect in the nonaqueous solvents of DMSO and CHB/decalin (*cf.* Materials and Methods) to rapidly assemble commercially available polymer latex colloids of a broad size range (0.1 to 1.2 μm) into ordered crystalline arrays that display reversible structural color in solution. Low-voltage (less than 3 V) dc electric fields are used to drive negatively charged polystyrene colloidal particles to the positively charged electrode surface fabricated from transparent indium tin oxide (ITO). The particles increase in density at the electrode surface until they self-assemble to form a thick ($\sim$20 μm) ordered crystal with close-packed structure. The self-assembled ordering, and thus the bulk structural color, is maintained while the dc electric field is applied. Then, upon removal of the dc electric field, the particles in the ordered crystals transition back into their disordered fluid phase and the bulk structural color thereby switches off. This paper thus demonstrates that the simple, rapid, and inexpensive method of electrophoretic deposition by dc electric fields can be applied to switch a colloidal suspension between its disordered and ordered states, thereby generating structural color that is reversible on demand.

RESULTS AND DISCUSSION

The self-assembly of colloids in the dc electric field device is demonstrated by the results of Figure 1 for the particular case of poly(methyl methacrylate) (PMMA) colloids suspended in CHB/decalin. We use a spacer to separate the two electrodes of the device so as to create a thin gap (120 μm, Figure 1a) in which the assembly occurs. The thin gap contributes to the rapid generation ($\sim$60 s) of colloidal assemblies. As shown in Figure 1b, the colloids are initially dispersed homogeneously between the electrode gap at 2.0 vol %. Application of a 2.0 V dc electric field leads to the electrophoretic motion of PMMA particles to the negatively charged electrode. Within a short period of time, the volume fraction of the particles at the substrate increases and they self-assemble into close-packed crystal structures (*cf.* Figure 1c). The resultant assemblies are 3D crystalline assembly structures as shown by the confocal micrograph of Figure 1d, which was acquired in a plane parallel to the electrode surface. The electrode surface is apparent at the image bottom.

In these experiments, the effect of the dc electric field on the colloid density is balanced by a gradient in the osmotic pressure of the colloidal suspension.[36] The gradient leads to high osmotic pressures at the electrode surface, and these high osmotic pressures correspond to an accumulation of colloids in the near electrode region. Hence, the region closest to the coverslip has a high particle volume fraction, which given a sufficient field strength and initial particle concentration can lead to a fluid−crystal transition. Away from (above) the electrode, the osmotic pressure decreases, along with the colloid volume fraction. As distance from the electrode increases, the volume fraction of the colloidal particles eventually drops below the fluid−crystal transition volume fraction. Hence, the assemblies are crystalline close to the electrode surface, while the particles transition from a crystalline to a disordered fluid state at a further distance, consistent with the image of Figure 1d, in which the bottom 20 μm of the electrophoretically deposited material is crystalline.

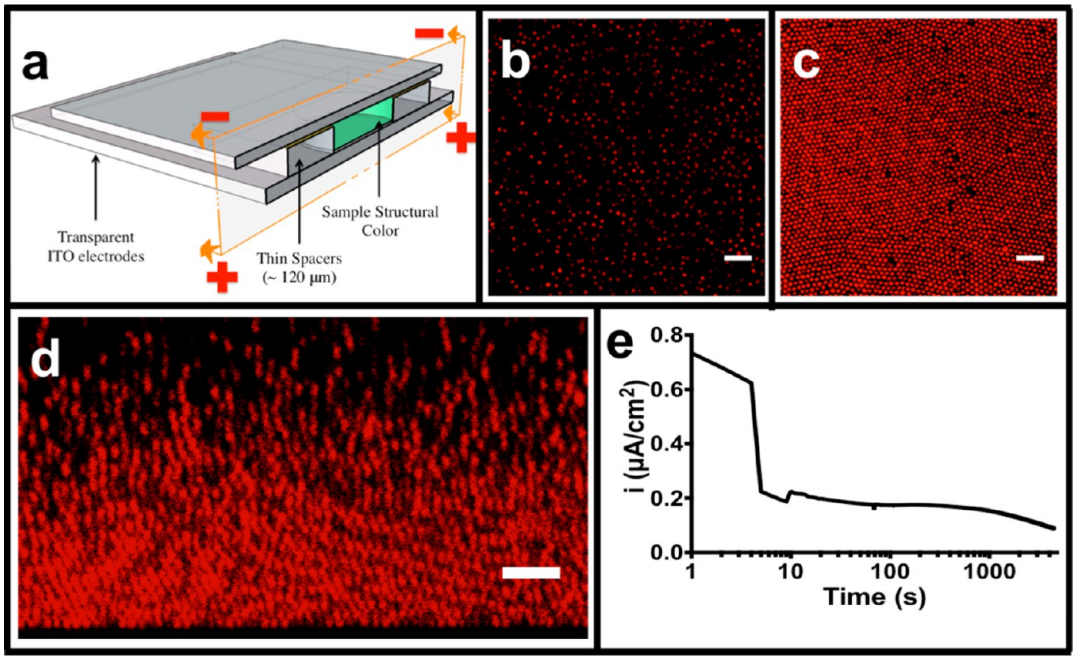

Figure 1. (a) Schematic of the electric field device. The electrode polarity is set based on the sign of the charge of the colloids used. (b) CLSM image of dispersed PMMA particles (700 nm in diameter) in the solvent CHB/decalin before application of the dc field. (c) Steady-state CLSM image of PMMA particle assembly structure at the electrode surface after application of a 2.0 V dc electric field. (d) Steady-state CLSM image of PMMA particle assembly taken in a plane perpendicular to the electrode surface after application of a 2.0 V dc electric field. Scale bars are 5 μm. (e) Current density as a function of time as measured in the electric field device for the assembly (b–d).

The electrochemical mechanism that drives dc electric field assembly has been discussed.[36] Briefly the application of a dc voltage leads to the reaction of residual dissolved species, such as water, oxygen, and possibly, in this case, the dissolved surfactant tetrabutylammonium chloride (TBAC), at the electrode surface. These reactions generate ion gradients that drive current flow. The time-dependent magnitude of the current is measured using a potentiostat (Autolab PGSTAT 128N) and is plotted in Figure 1e. There is a monotonic decrease over time in the current generated in the device due to consumption of residual reactants over time. This change in current density implies a reduction in the rate of reaction over time, due to reactant consumption.[36] The measured current is directly proportional to the electric field generated in the device: $E = i/\psi_0$, where E is the electric field, i is the measured current density, and ψ_0 is the solvent conductivity. This electric field drives the electrophoretic motion of charged colloids toward the oppositely charged electrode. It is this electric field that is balanced by the osmotic pressure gradient and is therefore responsible for the crystalline structure observed in Figure 1c,d. The gradient in osmotic pressure in the fluid leads to a maximum in the osmotic pressure at the electrode surface. The highest osmotic pressure is therefore generated at the electrode surface by the current flowing in the device (rather than generated by the electrode itself). In the subsequently reported experiments, we apply a dc voltage (up to 3 V) that is sufficient to generate the current needed to drive the colloidal particles into crystalline assemblies. We note that this assembly mechanism does not involve field-induced particle polarization; the currents and effective electric fields generated in the dc electric field device are not sufficient to appreciably polarize the colloidal particles.[37]

Figure 2 shows imaging and light scattering results of dc electric field induced assembly of polystyrene (PS) colloidal spheres of various diameters, suspended in DMSO. Using dynamic light scattering, the change in the diameter of the PS particles when suspended in DMSO was measured to be less than 4% of the value reported by the manufacturer. All the experiments were performed for colloidal suspensions of 2% initial volume fraction. The PS colloids are undyed, so that the observation of structural color is not complicated by accompanying fluorescence. We thus use reflection confocal laser scanning microscopy (CLSM) to visualize the particle assemblies produced at the electrode surface. Figure 2a shows the assembly of 1.2 μm diameter polystyrene particles suspended in DMSO upon application of a 2.0 V dc electric field. The image shows overall crystalline order, with grains of dimension ~20 μm. Light-scattering diffraction measurements were performed using a 632.8 nm laser, and the 6-fold diffraction pattern is shown in the inset image. The measured scattering angle of the diffraction pattern, which is an indication of the spacing of the close-packed crystal as shown later, is 18.4 $\pm$ 1.5° at this

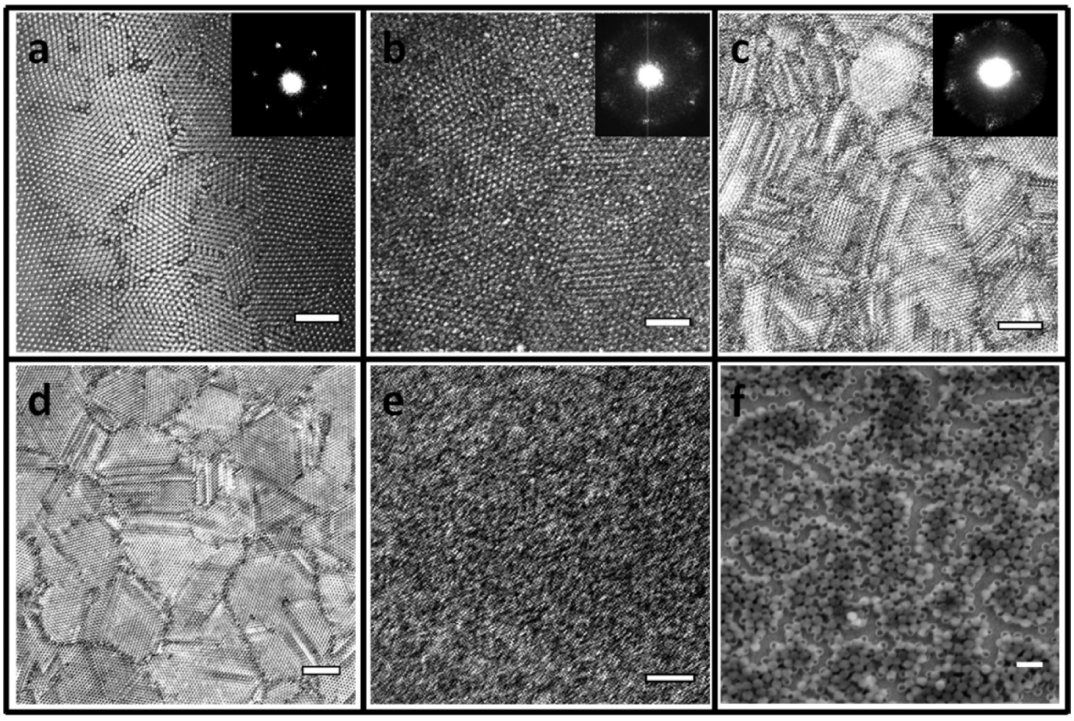

Figure 2. (a–e) CLSM reflection channel image of dc electric field assembly at the electrode surface. Insets for a–c are 6-fold diffraction experiments by small-angle light scattering. All experiments use DMSO as a solvent. (a) 1.2 μm PS colloids; (b) 0.95 μm PS colloids; (c) 0.50 μm PS colloids; (d) 0.40 μm PS colloids; (e) 0.29 μm colloids. Scale bars are 5 μm. (f) Scanning electron microscopy image of 0.11 μm PS particles in DMSO. Scale bar is 0.5 μm. These images were acquired after the field had been applied for ~5 min.

condition. Figure 2b shows similar results, but now for 0.96 μm diameter PS colloids. This crystalline assembly, with grain boundaries again apparent, was obtained on application of a voltage of ~2.25 V. A 6-fold diffraction pattern is observed at a scattering angle of 24.4 ± 1.5° (Figure 2b inset). Likewise, Figure 2c shows the crystalline assembly of 0.50 μm diameter PS colloids as obtained upon application of a 2.65 V dc electric field. The inset shows the 6-fold diffraction pattern observed for the case of a 532 nm laser. For this wavelength, the measured diffraction angle is 37.5 ± 2.2°. The reported diffraction angles account for refraction of the diffracted light at the device to air interface (*cf.* Materials and Methods).

Figure 2d,e reports the assembly of 0.40 and 0.29 μm diameter PS particles at an applied voltage of 2.75 and 2.9 V, respectively. Because of their small size, light-scattering experiments do not show 6-fold diffraction patterns for these assemblies. As we describe later (*cf.* Figure 3), this observation is consistent with the optical properties of these samples. Finally, Figure 2f shows the assembly of 0.11 μm diameter carboxylate-stabilized polystyrene particles from an initial volume fraction of 0.01 vol %. These particles were assembled at a voltage of 2.9 V using the alternate device geometry over 24 h (*cf.* Materials and Methods). Crystal domains are observed in these samples as opposed to multiple crystalline layers observed in the other samples. This difference is likely due to postassembly fluid flows generated during drying of the sample that caused deterioration in crystal quality. (Drying was required for SEM characterization of these small particle samples.)

Figure 2 therefore demonstrates the capability of the dc electric field device to self-assemble nanometer- to micrometer-sized particles into ordered arrays. The results show that high-quality assemblies are realized by means of different applied dc voltages, with these voltages varying from 2.0 V for the largest particle size to 2.9 V for the smallest particle size. The average current density (*i*) for these experiments ranges from 68.7 μA/cm^2 (2.9 V applied field) to 3.3 μA/cm^2 (2 V applied field). These different applied voltages lead to different current profiles and different driving forces on the colloids.[36] Broadly, as the particle size is decreased, a larger applied voltage is needed to generate the current density that establishes an electric field strength that is sufficiently large to create the colloidal assembly.

The physical origin of the higher voltages and current densities required for ordering at small particle size is the balance of the convective effect of the applied field and the randomizing effect of Brownian motion. Because the colloidal diffusivity is inversely related to the particle size, a higher external field strength is needed at small size to balance the randomizing effect of this enhanced diffusivity and therefore generate the high, near wall volume fractions that lead to ordering. The primary advantage of the dc electric field device is that small changes in voltage lead to

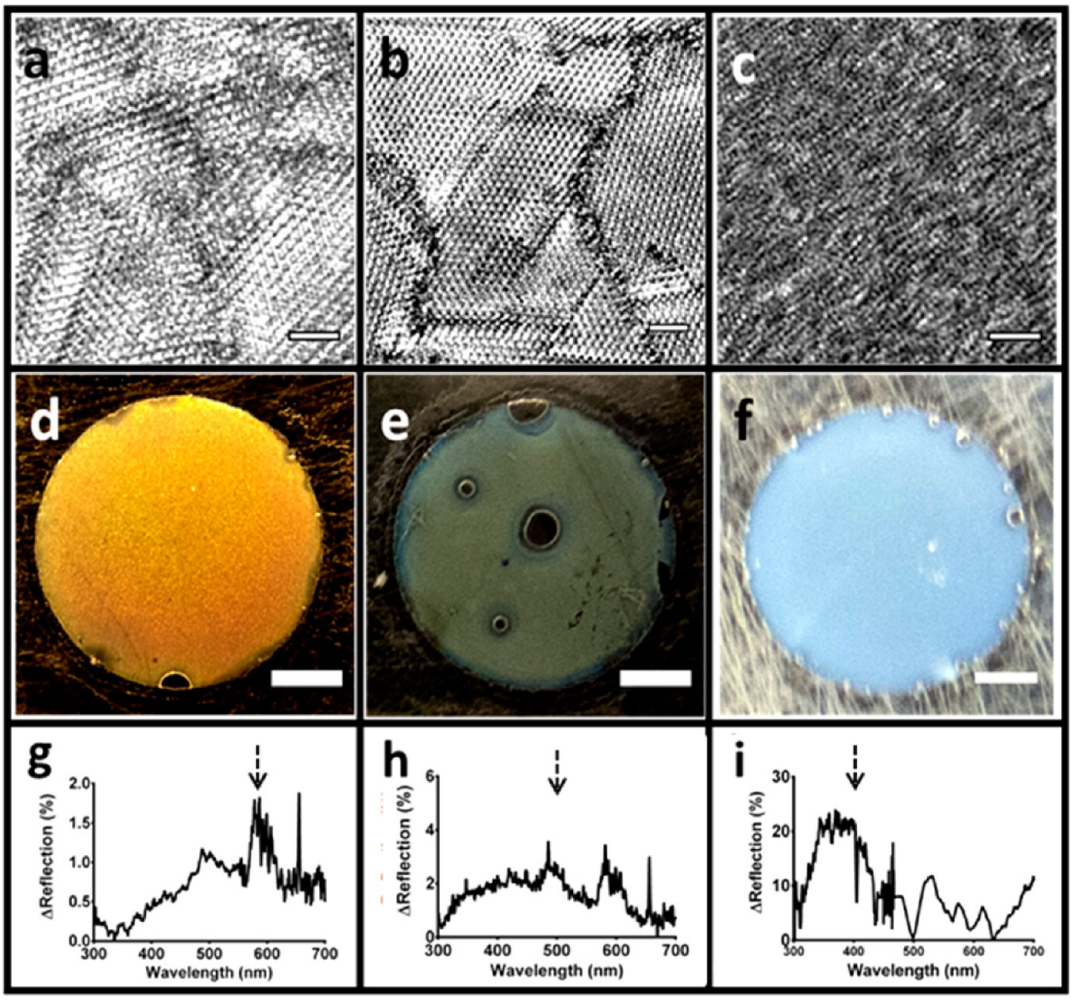

Figure 3. (a−c) CLSM reflection channel images of the dc electric field induced assembly of 0.50, 0.40, and 0.29 μm sized particles, respectively. Scale bars are 2 μm. (d−f) Bulk structural color observed for the 0.50, 0.40, and 0.29 μm sized particles, respectively. These images were acquired by a point and shoot digital camera (Olympus XZ-1). Scale bars are 2 mm. (g−i) Spectrophotometry of the structural color assemblies as observed for 0.50, 0.40, and 0.29 μm sized particles, respectively. The spectrophotometer is operating in a back reflection mode, and the measured waveforms were subtracted from a baseline (measured for the disordered fluid with the electric field turned off). The data are passed through a simple moving average with a width equivalent to 1.5 nm to filter instrument noise, and the origin has been adjusted to the visible spectrum and the minimum signal measured. The theoretically predicted Bragg peaks, $\lambda_{the,D}$, from Table 1, are denoted as arrows.

large increases in the current generated (and thus the effective electric field generated) in the system.[38] Thus, we observe the ordered assemblies of particles ranging from 0.1 to 1.2 μm in Figure 2 even given the relatively small changes in voltage. We also observe that the grain size of the observed assemblies remains relatively constant for different particle sizes (except for the 0.1 μm assembly for reasons described earlier).

Figure 3 reports that PS colloidal particles of intermediate diameter display visible structural color. The structural color colloidal crystals are formed from colloids of diameter 0.50, 0.40, and 0.29 μm. Figure 3a,b,c displays CLSM reflection channel images for these respective particle sizes. The images show crystalline order and were acquired after application of a dc electric field (*cf.* Figure 2). The samples are initially colorless on vertical incidence and reflection of white light. Figure 3d−f shows the orange, green, and blue structural color observed for the 0.50, 0.40, and 0.29 μm diameter PS samples, respectively, after the electrophoretic deposition. The structural color produced by the assembly method is analyzed by reflection spectrophotometry, as reported in Figure 3g−i. The sample with a bulk structural color of orange shows a reflectance peak at ~0.6 μm, the green sample has a peak at ~0.51 μm, and the blue sample has a peak at ~0.4 μm.

We corroborate the formation of dc electric field assisted crystal assemblies by comparing the observed diffraction patterns (Figure 2) and the observation of visible structural color (Figure 3d−f) with theoretical predictions. First, the observed diffraction angles, reported above, are related to the scattering wave vector through its definition:

$$q_{expt} = \frac{4\pi n_{solvent}}{\lambda_0} \sin\left(\frac{\theta}{2}\right) \quad (1)$$

TABLE 1. Comparison of Measurements of Light-Scattering Diffraction and Reflectance to Predictions of Bragg's Law[a]

d (nm)	q_{expt} (μm^{-1})	$q_{the,D}$ (μm^{-1})	$q_{the,ND}$ (μm^{-1})	$\lambda_{the,D}$ (μm)	$\lambda_{the,ND}$ (μm)
290				0.43 (m=3)	0.36 (m=2)
400				0.53 (m=3)	0.50 (m=2)
500	11.2 ± 1.2	9.6	14.5	0.63 (m=3)	0.62 (m=2)
960	6.2 ± 0.7	5.8	7.6		
1200	4.7 ± 0.7	4.8	6.0		

[a] Here, d is the particle diameter. q_{expt} is the experimentally measured structure factor. $q_{the,D}$ and $q_{the,ND}$ are the theoretical structure factor computed for the two cases of inclusion and exclusion of the Debye layer thickness in the estimation of the Bragg spacing. $\lambda_{the,D}$ and $\lambda_{the,ND}$ are the theoretical expected wavelength computed for the same two cases of Debye layer thickness included or not included.

Here q_{expt} is the experimentally measured diffraction scattering wave vector, λ_0 is the wavelength of incident light in a vacuum, $n_{solvent}$ is the solvent refractive index, and θ is the measured angle of diffraction (*cf.* Materials and Methods). The experimentally measured diffraction scattering vectors are reported in Table 1.

We apply the diffraction theory for close-packed crystals of Loose and Ackerson[39] to compare to the experiments. The reflection CLSM images of Figures 2 and 3 show close-packed layers parallel to the electrode surface. In this configuration, for an incident beam normal to the close packed layers,

$$q_{theory} = \frac{2\pi}{\sigma}\sqrt{\frac{4}{3}} \quad (2)$$

where q_{theory} is the theoretical scattering vector and σ is the separation between the particles. We use two formulations for σ. The first includes the effect of the Debye layer around the PS particles, and the second neglects the presence of a Debye layer. We expect these two cases may serves as limits on the observations. In the former case, σ is given by $\sigma = (1/k)\ln(\alpha/\ln(\alpha/...))$, where $\alpha = \pi\varepsilon\varepsilon_0\zeta^2 d^2 k e^{dk}(k_B T)^{-1}$, and we denote the theoretical scattering vector as $q_{the,D}$.[40] Here, ε is the dielectric constant of DMSO, ε_0 is permittivity of free space, ζ is the zeta potential, κ^{-1} is the Debye layer thickness, k_B is the Boltzmann constant, T is the temperature, and d is the diameter of the PS particles. In the latter case, σ is taken to be equal to the diameter of the particles, and we denote this theoretical scattering vector as $q_{the,ND}$. Table 1 indicates a good agreement with the experimental and theoretical scattering vectors. Specifically, q_{expt} is in better agreement with $q_{the,D}$ (mean deviation of 9% across all samples) than with $q_{the,ND}$ (mean deviation of 16% across all samples). This comparison establishes that the observed diffraction patterns are Bragg peaks generated by the close-packed crystal structure, as imaged with reflection CLSM. The separation between the colloidal particles is greater than the diameter of the particles, thereby including an effect of the finite Debye layer thickness. The finite Debye layer thickness leads to an increase in the separation between particles in a close-packed assembly, with a resultant effect on the location of the diffraction peaks.

Second, to connect the crystal formation by colloidal particles of size less than 0.5 μm to their observed structural color response, the wavelength of the structural color exhibited by the electrophoretically deposited colloidal crystal can also be predicted. As discussed, for example, in Fudouzi and Xia,[41] for the reflection geometry, the relationship between the wavelength of the reflected radiation is related to the spacing between the close-packed layers according to

$$m\lambda_{theory} = 2\sigma_{hkl}[n_{eff}^2 - \sin^2(\theta_{reflection})]^{1/2} \quad (3)$$

where m is the order of diffraction, λ_{theory} is the reflected wavelength, $\theta_{reflection}$ is the angle of incidence of light relative to the normal (here equal to 180°), σ_{hkl} is the spacing between the close-packed fcc crystal layers, given by $\sigma_{hkl} = 0.82\sigma$, and n_{eff} is the effective refractive index (*cf.* Materials and Methods). σ_{hkl} is similarly computed for the cases of inclusion and exclusion of the Debye layer as discussed earlier, and the predicted wavelengths are $\lambda_{the,D}$ and $\lambda_{the,ND}$, respectively, as included in Table 1. As is evident in eq 3, different wavelengths of light are scattered at different angles when white light is incident on the colloidal crystal. In Figure 3d–f, white light is incident on the sample, and the resulting structural color is imaged perpendicular to close-packed planes of the crystal, which are parallel to the electrode surface. The predictions of eq 3 are in good agreement with the visually observed structural color at an order of diffraction of m = 3 when the effect of the finite Debye layer is included and m = 2 when the presence of a Debye layer is not included in the theoretical calculations. Table 1 reports the predictions of eq 3 within the visible spectrum. (We note that for the first-order of diffraction (m = 1), reflected wavelengths are not in the visible region.) Although the order of the diffraction observed in Figure 3d–f is unclear because of the uncertain effect of the finite Debye layer and the breadth of the observed spectrophotometric spectrum, the observation of higher order diffraction has been reported previously.[42–44] In Figure 3g–i, the predicted diffraction peaks computed by including the effect of the Debye layer are indicated with arrows for the PS particles of diameter 0.5, 0.4, and 0.29 μm, respectively. Taken together, the congruence of the diffraction and reflection predictions with the measured light scattering and spectrophotometry strongly supports the origin of the optical observations as being the closed-packed ordering observed in the optical micrographs.

These reported electrophoretic deposition results are all for fluid suspensions, which admits the possibility of reversibility. Figure 4 shows the reversibility of

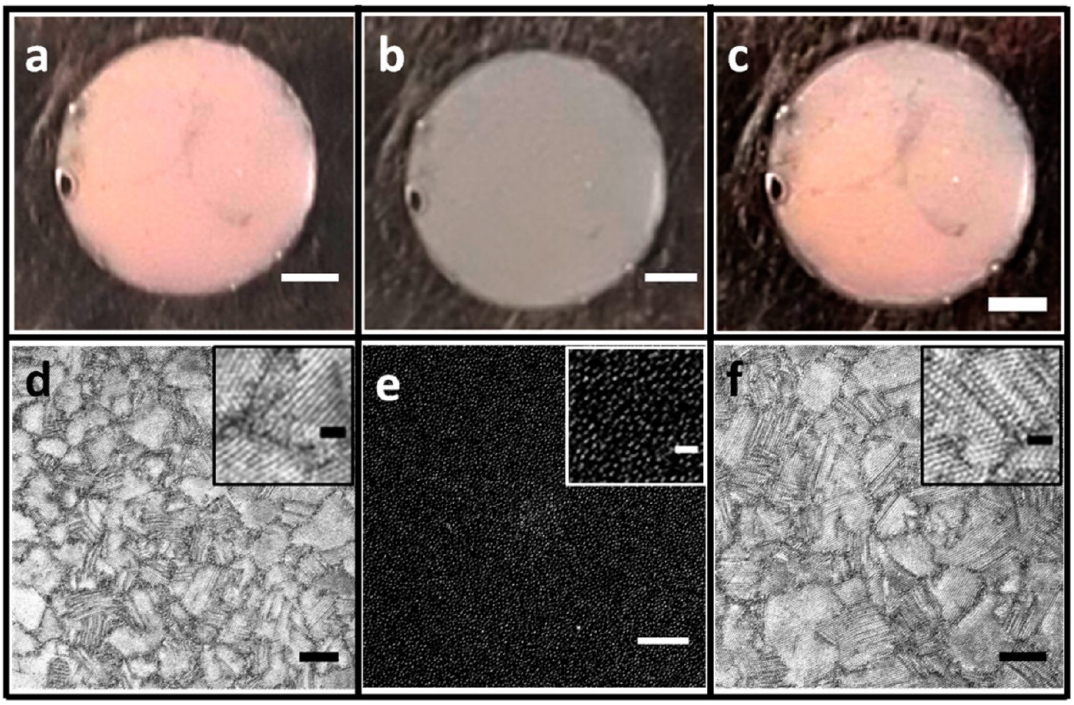

Figure 4. (a) Reversible structural color obtained for 0.50 μm particles on application of a 2.65 V dc electric field. (b) Bulk color of the sample on removal of the dc electric field after 30 s. (c) Regeneration of structural color on application of a dc electric field for 1 min. (d) CLSM reflection channel image of a colloidal suspension on application of a 2.65 V dc electric field. (e) CLSM reflection channel image of a colloidal suspension after removal of a dc electric field. (f) CLSM reflection channel image of a colloidal suspension on reapplication of a 2.65 V dc electric field. Scale bars are (a−c) 2 mm and (d−f) 10 μm.

the structural color for the particular case of 0.5 μm diameter particles. Reversibility was generated by switching the dc electric field on and off. Application of a 2.65 V dc electric voltage for 1 min generated structural color (Figure 4a). Removal of the external dc electric voltage (0 V) led to a loss in the bulk structural color in approximately 30 s (Figure 4b). Reapplication of the external dc electric voltage (2.65 V) regenerated the structural color in about 1 min (Figure 4c). This functional change in the structural color is caused by microstructural changes in the colloidal assembly, as indicated by the accompanying CLSM micrographs of Figure 4d−f. Figure 4d shows the CLSM reflection channel image of the close-packed assembly obtained on application of the dc electric field. Removal of the dc electric field leads to the generation of a disordered fluid phase (Figure 4e). This change in the microstructure of the sample is fast (~5 s) because the Brownian motion of the colloidal particles rapidly promotes disorder in the sample. Reapplication of the external field leads to re-formation of the close-packed assemblies, and this change accompanies the regeneration of the bulk structural color (*cf.* Figure 4f). This reversibility is reproducible and has been tested at least six times on the same sample.

CONCLUSION

We have used a direct current electric field method to produce ordered colloidal assemblies from colloids varying in size from 0.1 to 1.2 μm. The crystallinity of the 3D assemblies was visualized using reflection confocal microscopy for micrometer-sized particles and scanning electron microscopy for nanosized particles. The assemblies displayed 6-fold diffraction symmetry at scattering vectors consistent with Bragg's law. Colloids of diameter 0.50, 0.40, and 0.29 μm assembled under dc fields into crystals with orange, green, and blue structural color. These colors were quantified by reflection spectrophotometry, and these results also are consistent with expectations based on the modified Bragg's equation. The formation of the crystallinity and structural color is reversible on fast time scales (~1 min). DC electric field assembly is thus a simple method to rapidly produce colloidal crystals of sufficient quality to generate diffraction and structural color that could potentially be useful for a variety of applications.

MATERIALS AND METHODS

Colloidal Particles. Polymer latex particles are suspended in organic solvents for assembly with dc electric fields. As discussed in the introduction, these organic solvents are selected to suppress electro-osmotic and electrohydrodynamic flows generated by the reaction of electrochemically decomposable solvents (such as water) that tend to limit assembly of planar structures. Two kinds of polymer latex are used. Most assembly

experiments use polystyrene colloids suspended in dimethyl sulfoxide. This system is used for all light-scattering, spectrophotometry, and structural color experiments. PS particles of a variety of different sizes (0.10, 0.29, 0.40, 0.50, 0.96, and 1.20 μm in diameter) were purchased in aqueous suspensions (Invitrogen Inc. and Bangs Laboratories). The colloids are carboxylate or sulfate stabilized, and the sign of their charge is negative. These suspensions are centrifuged at 5000*g* for 1 h to separate the particles from the solvent (one transfer). The solvent is replaced by DMSO for dc electric field assembly experiments. The Debye length for the PS/DMSO system is calculated to be 50 nm.

In addition, some experiments are performed with PMMA particles suspended in CHB/decalin. Because this colloid−solvent system is refractive index matched, confocal microscopy can be used to image deep into the colloidal crystals and thereby confirm that the method yields a 3D crystalline assembly. The PMMA colloids with Nile Red dye incorporated are synthesized with a polyhydroxystearic acid (PHSA) stabilizer using literature methods.[9,45] The synthesized particles are 0.70 ± 0.08 μm in diameter. To acquire sufficient charge for electrophoretic deposition in the refractive index matched solvent of CHB/decalin, the stabilizer concentration on the surface was increased by the following additional synthetic step:[46] 1.0 g of the synthesized particles were suspended in 20 mL of hexane (Sigma-Aldrich). Then, 1.0 g of PHSA was added to the solution. Finally, 0.01 g of the initiator azobis(isobutyronitrile) was added and dissolved in solution. This solution was heated in a three-neck flask at 60−70 °C for approximately 2 h. The particles were then hexane washed by centrifugation at least five times and dried subsequently for 1 day. The particles are then dispersed in cyclohexyl bromide (Sigma-Aldrich) and decalin (Sigma-Aldrich) (66:34 volume percent to create refractive index matched particle and solvent systems). A 100 μM tetrabutylammonium chloride salt is also added to the system to increase the conductivity of the solvent. The sign of the charge of the PMMA colloids is positive. Therefore, the electrode polarity for these experiments was opposite of that for the experiments with the PS colloids.

Direct Current Electric Field Device. Two device geometries are used for the electrophoretic assembly by application of dc electric fields. A sectional view of the primary dc electric field device is shown in Figure 1a. The device is made up of ITO-coated transparent electrode slides. These slides are separated by a thin, closed spacer (120 μm thick, Grace Bio-Laboratories imaging spacers, GBL654002), with the ITO conductive half of the slide facing inward. The colloidal suspension is placed within the spacer and is in contact with the two electrode slides. The slides are glued to T2 thermocouple wires (Goodfellow Inc.) that are connected to a dc electric voltage source. Voltages of up to 3.0 V are applied across the device using a dc electric voltage generator (Autolab PGSTAT 128N).

Nanoparticles are assembled using an alternate device geometry to facilitate *ex situ* visualization by scanning electron microscope (SEM). The alternate device geometry consists of two parallel ITO-coated electrode coverslips separated by an open spacer (1 mm thick) that are dipped in a large volume of the colloidal suspension (~100 mL). The spacer is made from microscope slides (Sigma-Aldrich) that are cut into smaller pieces (1 cm × 3 cm) and applied to each of the electrodes using UV-curable glue (Light Weld, Dymax Corporation). Voltages of up to 3 V are applied across the device using a dc electric voltage generator (HP). The device is removed from the colloidal suspension, and the slides are separated from the spacer using a sharp blade. These slides are subsequently imaged using an SEM.

Confocal Laser Scanning Microscopy. The electric field device was placed on the stage of a Nikon A1r CLSM with a 100× (NA = 1.4) objective. The positive polarity electrode was positioned directly above the objective for experiments with the PS colloids. Electrode polarity for PMMA colloids was reversed. The CLSM was used in fluorescent mode to image dyed PMMA colloids in CHB/decalin. The reflection mode was used to image the undyed PS colloids in DMSO. A 488 nm wavelength laser was used to scan the samples for both fluorescence (emission spectrum: 490−550 nm) and reflection imaging. A variety of pixel sizes were scanned for the various CLSM images in this paper (17.92−124.46 nm/pixel). Images were 512 × 512 pixel or 2048 × 2048 pixel in size.

Scanning Electron Microscopy. SEM imaging was used to image nanoparticles that could not be resolved by CLSM. The electric field device is removed from the particle suspension and allowed to air-dry for approximately 1 h. The positive and negative electrodes are then separated and cut into small pieces using a sharp blade. These pieces are affixed to SEM stubs using carbon black conductive adhesives and imaged using an SEM (Phillips XL-30 field emission gun) operating at 15 kV.

Light-Scattering Diffraction. Diffraction from the field-assisted assemblies was probed by laser light scattering.[47] Briefly, a laser of wavelength 632.8 nm (Melles Griot Inc.) with a $1/e^2$ diameter of 0.71 mm was expanded, spatially filtered, and subsequently focused with a converging lens. The reduced beam was the incident light on the specimen. Diffraction patterns from the sample were captured on a translucent screen placed behind the sample. The diffraction patterns were imaged using a wide-angle lens (Thor Laboratories) mounted on a CCD camera (resolution 1390 × 1024 pixels with pixel size 6.4 μm × 6.4 μm, PixelFly, Cooke Corporation, Auburn Hills, MI, USA) located at a distance of 10 cm from the screen. The angle of diffraction (θ) was obtained by measuring the distance of the screen from the sample and the diameter of the diffraction ring. Specifically, a Snell's law correction to account for the cell/air boundary was applied to the apparent angle computed from these dimensions. The resulting angle of diffraction, θ, was used to calculate the measured diffraction scattering vector for comparison to theory. For these experiments in the polystyrene DMSO system, the solvent refractive index, n_{DMSO}, is 1.48, the particle refractive index, n_{PS}, is 1.59, and the effective refractive index of the dense sediments, n_{eff}, is 1.53. (Here, $n_{eff} = \phi_{PS}n_{PS} + \phi_{DMSO}n_{DMSO}$, where ϕ_{PS} is the particle volume fraction and ϕ_{DMSO} is the solvent volume fraction.) This device configuration was used for assemblies produced from particles greater than 0.6 μm in diameter. For particles of diameter 0.6 μm < d < 0.4 μm, a laser source of 532 nm ($1/e^2$ diameter of 0.32 mm) was used (Compass 315M, Coherent Inc.).

Spectrophotometry. Structural color is measured using a fiber optic spectrophotometer (USB 2000, Ocean Optics Inc.). The wavelength range probed is from 300 to 700 nm. The probe is placed normal to the sample surface to ensure that the angle of incidence and reflection are coincident. The reflection spectrum of the sample measured before application of the electric field is taken as the background contribution and is subtracted from the reflection spectrum of the assembled specimen.

Disclosure: Any opinions, findings, and conclusions or recommendations expressed in this publication are those of the authors and do not necessarily reflect the views of the DOD.

Conflict of Interest: The authors declare no competing financial interest.

Acknowledgment. This work was supported by the U.S. Army Research Office under Grant Award No. W911NF-10-1-0518.

REFERENCES AND NOTES

1. Kolle, M.; Salgard-Cunha, P. M.; Scherer, M. R. J.; Huang, F.; Vukusic, P.; Mahajan, S.; Baumberg, J. J.; Steiner, U. Mimicking the Colourful Wing Scale Structure of the Papilio Blumei Butterfly. *Nat. Nanotechnol.* **2010**, *5*, 511–515.
2. McNamara, M. E.; Briggs, D. E. G.; Orr, P. J.; Noh, H.; Cao, H. The Original Colours of Fossil Beetles. *Proc. R. Soc. B* **2012**, *279*, 1114–1121.
3. Mäthger, L. M.; Denton, E. J.; Marshall, N. J.; Hanlon, R. T. Mechanisms and Behavioural Functions of Structural Coloration in Cephalopods. *J. R. Soc., Interface* **2009**, *6*, S149–S163.
4. Geissler, M.; Xia, Y. Patterning: Principles and Some New Developments. *Adv. Mater.* **2004**, *16*, 1249–1269.
5. Pusey, P. N.; Van Megen, W. Phase Behaviour of Concentrated Suspensions of Nearly Hard Colloidal Spheres. *Nature* **1986**, *320*, 340–342.

6. Lee, W.; Chan, A.; Bevan, M. A.; Lewis, J. A.; Braun, P. V. Nanoparticle-Mediated Epitaxial Assembly of Colloidal Crystals on Patterned Substrates. *Langmuir* **2004**, *20*, 5262–5270.
7. Jensen, K. E.; Pennachio, D.; Recht, D.; Weitz, D. A.; Spaepen, F. Rapid Growth of Large, Defect-Free Colloidal Crystals. *Soft Matter* **2013**, *9*, 320–328.
8. Jiang, P.; McFarland, M. J. Large-Scale Fabrication of Wafer-Size Colloidal Crystals, Macroporous Polymers and Nanocomposites by Spin-Coating. *J. Am. Chem. Soc.* **2004**, *126*, 13778–13786.
9. Shereda, L. T.; Larson, R. G.; Solomon, M. J. Local Stress Control of Spatiotemporal Ordering of Colloidal Crystals in Complex Flows. *Phys. Rev. Lett.* **2008**, *101*, 038301.
10. Prevo, B. G.; Velev, O. D. Controlled, Rapid Deposition of Structured Coatings From Micro- and Nanoparticle Suspensions. *Langmuir* **2004**, *20*, 2099–2107.
11. Kleinert, J.; Kim, S.; Velev, O. D. Electric-Field-Assisted Convective Assembly of Colloidal Crystal Coatings. *Langmuir* **2010**, *26*, 10380–10385.
12. Jiang, P.; Bertone, J. F.; Hwang, K. S.; Colvin, V. L. Single-Crystal Colloidal Multilayers of Controlled Thickness. *Chem. Mater.* **1999**, *11*, 2132–2140.
13. Vlasov, Y. A.; Bo, X.-Z.; Sturm, J. C.; Norris, D. J. On-Chip Natural Assembly of Silicon Photonic Bandgap Crystals. *Nature* **2001**, *414*, 289–293.
14. Furumi, S.; Fudouzi, H.; Sawada, T. Self-Organized Colloidal Crystals for Photonics and Laser Applications. *Laser Photonics Rev.* **2010**, *4*, 205–220.
15. Fudouzi, H.; Sawada, T. Photonic Rubber Sheets with Tunable Color by Elastic Deformation. *Langmuir* **2006**, *22*, 1365–1368.
16. Lee, K.; Asher, S. A. Photonic Crystal Chemical Sensors: pH and Ionic Strength. *J. Am. Chem. Soc.* **2000**, *122*, 9534–9537.
17. Arsenault, A. C.; Puzzo, D. P.; Manners, I.; Ozin, G. A. Photonic-Crystal Full-Colour Displays. *Nat. Photonics* **2007**, *1*, 468–472.
18. Lumsdon, S. O.; Kaler, E. W.; Velev, O. D. Two-Dimensional Crystallization of Microspheres by a Coplanar Ac Electric Field. *Langmuir* **2004**, *20*, 2108–2116.
19. Forster, J. D.; Park, J.-G.; Mittal, M.; Noh, H.; Schreck, C. F.; O'Hern, C. S.; Cao, H.; Furst, E. M.; Dufresne, E. R. Assembly of Optical-Scale Dumbbells into Dense Photonic Crystals. *ACS Nano* **2011**, *5*, 6695–6700.
20. Mukhija, D.; Solomon, M. J. Nematic Order in Suspensions of Colloidal Rods by Application of a Centrifugal Field. *Soft Matter* **2011**, *7*, 540–545.
21. Ahniyaz, A.; Sakamoto, Y.; Bergström, L. Magnetic Field-Induced Assembly of Oriented Superlattices From Maghemite Nanocubes. *Proc. Natl. Acad. Sci. U.S.A.* **2007**, *104*, 17570–17574.
22. Ge, J.; He, L.; Goebl, J.; Yin, Y. Assembly of Magnetically Tunable Photonic Crystals in Nonpolar Solvents. *J. Am. Chem. Soc.* **2009**, *131*, 3484–3486.
23. Ding, T.; Song, K.; Clays, K.; Tung, C. Fabrication of 3d Photonic Crystals of Ellipsoids: Convective Self-Assembly in Magnetic Field. *Adv. Mater.* **2009**, *21*, 1936–1940.
24. Kim, Y.; Shah, A. A.; Solomon, M. J. Spatially and Temporally Reconfigurable Assembly of Colloidal Crystals. *Nat. Commun.* **2014**, 10.1038/ncomms4676.
25. Sullivan, M. T.; Zhao, K.; Hollingsworth, A. D.; Austin, R. H.; Russel, W. B.; Chaikin, P. M. An Electric Bottle for Colloids. *Phys. Rev. Lett.* **2006**, *96*, 015703.
26. Yethiraj, A.; Thijssen, J. H.; Wouterse, A.; van Blaaderen, A. Large-Area Electric-Field-Induced Colloidal Single Crystals for Photonic Applications. *Adv. Mater.* **2004**, *16*, 596–600.
27. Gong, T.; Wu, D. T.; Marr, D. W. M. Electric Field-Reversible Three-Dimensional Colloidal Crystals. *Langmuir* **2003**, *19*, 5967–5970.
28. Juárez, J. J.; Bevan, M. A. Interactions and Microstructures in Electric Field Mediated Colloidal Assembly. *J. Chem. Phys.* **2009**, *131*, 134704.
29. Böhmer, M. *In Situ* Observation of 2-Dimensional Clustering During Electrophoretic Deposition. *Langmuir* **1996**, *12*, 5747–5750.
30. Giersig, M.; Mulvaney, P. Preparation of Ordered Colloid Monolayers by Electrophoretic Deposition. *Langmuir* **1993**, *9*, 3408–3413.
31. Trau, M.; Saville, D. A.; Aksay, I. A. Field-Induced Layering of Colloidal Crystals. *Science* **1996**, *272*, 706–709.
32. Dassanayake, U.; Fraden, S.; Van Blaaderen, A. Structure of Electrorheological Fluids. *J. Chem. Phys.* **2000**, *112*, 3851–3858.
33. Trau, M.; Saville, D. A.; Aksay, I. A. Assembly of Colloidal Crystals at Electrode Interfaces. *Langmuir* **1997**, *13*, 6375–6381.
34. Solomentsev, Y.; Böhmer, M.; Anderson, J. L. Particle Clustering and Pattern Formation during Electrophoretic Deposition: A Hydrodynamic Model. *Langmuir* **1997**, *13*, 6058–6068.
35. Rogach, A. L.; Kotov, N. A.; Koktysh, D. S.; Ostrander, J. W.; Ragoisha, G. A. Electrophoretic Deposition of Latex-Based 3d Colloidal Photonic Crystals: A Technique for Rapid Production of High-Quality Opals. *Chem. Mater.* **2000**, *12*, 2721–2726.
36. Shah, A. A.; Kang, H.; Kohlstedt, K. L.; Ahn, K. H.; Glotzer, S. C.; Monroe, C. W.; Solomon, M. J. Liquid Crystal Order in Colloidal Suspensions of Spheroidal Particles by Direct Current Electric Field Assembly. *Small* **2012**, *8*, 1551–1562.
37. Jones, T. B.; Jones, T. B. *Electromechanics of Particles*; Cambridge University Press, 2005.
38. Bard, A. J.; Faulkner, L. R. *Electrochemical Methods: Fundamentals and Applications*; Wiley: New York, 1980.
39. Loose, W.; Ackerson, B. J. Model Calculations for the Analysis of Scattering Data from Layered Structures. *J. Chem. Phys.* **1994**, *101*, 7211.
40. Russel, W. B.; Saville, D. A.; Schowalter, W. R. *Colloidal Dispersions*; Cambridge University Press, 1992.
41. Fudouzi, H.; Xia, Y. Colloidal Crystals with Tunable Colors and Their Use as Photonic Papers. *Langmuir* **2003**, *19*, 9653–9660.
42. Dorado, L. A.; Depine, R. A.; Lozano, G.; Míguez, H. Interplay between Crystal-Size and Disorder Effects in the High-Energy Optical Response of Photonic Crystal Slabs. *Phys. Rev. (Sect.) B* **2007**, *76*, 245103.
43. Nair, R. V.; Vijaya, R. Observation of Higher-Order Diffraction Features in Self-Assembled Photonic Crystals. *Phys. Rev. (Sect.) A* **2007**, *76*, 053805.
44. Kim, S.; Seo, Y. G.; Cho, Y.; Shin, J.; Gil, S. C.; Lee, W. Optimization of Emulsion Polymerization for Submicron-Sized Polymer Colloids towards Tunable Synthetic Opals. *Bull. Korean Chem. Soc.* **2010**, *31*, 1891–1896.
45. Antl, L.; Goodwin, J. W.; Hill, R. D.; Ottewill, R. H.; Owens, S. M.; Papworth, S.; Waters, J. A. The Preparation of Poly (Methyl Methacrylate) Latices in Non-Aqueous Media. *Colloids Surf.* **1986**, *17*, 67–78.
46. Zhang, Z.; Pfleiderer, P.; Schofield, A. B.; Clasen, C.; Vermant, J. Synthesis and Directed Self-Assembly of Patterned Anisometric Polymeric Particles. *J. Am. Chem. Soc.* **2010**, *133*, 392–395.
47. Fuller, G. G. *Optical Rheometry of Complex Fluids*; Oxford University Press: New York, 1995.